DUAL-LAYER EBG STRUCTURES FOR LOW-PROFILE "BENT" MONOPOLE ANTENNAS

Tangjie Yuan[1], Habiba Hafdallah Ouslimani[1, *], Alain C. Priou[1], Guillaume Lacotte[2], and Gérard Collignon[2]

[1]Waves Material and Systems Group, Energetic Mechanic Electromagnetic Lab, University Paris-Ouest Nanterre-La Défense, LEME (EA-4416) 50 rue de Sèvres, Ville d'Avray 92410, France

[2]INEO Défense, Route Militaire Nord-ZA Louis Bréguet, CS 80526, Velizy Villacoublay 78140, France

Abstract—We propose in this paper the design, realization and experimental characterization of a low-profile metamaterial "bent" monopole antenna with a total height of $0.027\lambda_0$ and a fractional bandwidth of 24.4% around 1.3 GHz. The metamaterial (MTM) structure is a dual-layer mushroom-like electromagnetic band gap (DL-EBG) conceived and optimized to improve the antenna's operating bandwidth. Moreover, a "Sabre-Type" antenna composed by two identical "bent" monopole metamaterial antennas placed on both sides of a composite thin slab material has been simulated and realized. The "sabre" antenna provides a vertically polarization and omnidirectional radiation patterns in the elevation plane while its radiation patterns are almost directional in the azimuth plane. A maximum gain of 8.7 dB is obtained by measurement at 1.45 GHz. A remarkable agreement is obtained between the measured and the simulated results.

1. INTRODUCTION

Low-profile antenna structures are subject to intensive development work during the past decade [1]. The main objective is to conceive compact antennas which could be integrated and imbedded into miniaturized systems [2]. Hence, there are different techniques [3–5] which allow a large reduction of the antenna dimensions, like using high permittivity substrates or meandering paths and fractal shapes antennas. However, they still present the disadvantage of narrow

antenna bandwidth and even important ohmic losses in the case of fractal shapes antennas. So presently, they are not suitable for aeronautic applications.

Sievenpiper et al. have developed High Impedance Surfaces (HIS) [6] with new electromagnetic properties, also called electromagnetic band gap (EBG) material. In front of an incident wave the structure operates as a perfect magnetic conductor (PMC) [7] with a reflection coefficient equal to +1 [8]. This property has been intensively investigated to design low-profile antennas [9–12].

For instance, in [9], a circularly polarized patch antenna was characterized using an artificial magnetic conductor ground plane (AMC_GP) and for comparison with a usual perfect electric conductor (PEC). A significant improvement has been obtained in the antenna matching input impedance and fractional bandwidth: from 1.5% to 9.6%. Then, in [10], a conventional 40 GHz patch element was surrounded by double and triple rows of EBG structure. The proposed antenna presents a fractional bandwidth up to 15%, a gain of 6 dB and a cross polar < -20 dB. Next, in [11], the patch antenna element is inserted at a certain distance inside the HIS material and acts as a patch-fed surface wave launcher. The HIS was composed of a periodic pattern of uniplanar metalized patches etched on a dielectric substrate backed by a PEC_GP. The antenna presents a monopole-like vertically polarized radiation patterns at 4.72 GHz with a bandwidth of 5.9% and a maximum gain of 5.6 dB. Finally, in [12], a "bent" monopole antenna based-on mushroom-like EBG_GP has been designed for beam switching for radar system at 4.32 GHz. In this case, the fabricated EBG_GP was composed of 8×8 unit cells with total size of $1.1\lambda_o \times 1.1\lambda_o \times 0.065\lambda_o$. The monopole element was placed at $0.02\lambda_o$ over the EBG-GP (air gap). Thus, a fractional bandwidth of 10.6% with a maximum gain of 7 dB is obtained at $29°$.

In this paper, we present a 24.4% relative bandwidth "bent" monopole MTM-based antenna for aeronautic applications. The designed antenna is based on a dual-layer mushroom-like electromagnetic bandgap, DL-EBG structure (called three-layer EBG structure or high impedance surface by D. Sevenpiper in his Ph.D. dissertation 1999) used as a ground plane with a total height of only $\lambda_o/36$. The antenna dimensions are $1.15\lambda_o \times 1.15\lambda_o \times 0.027\lambda_o$.

A comparative study (Section 3) has been performed between two "bent" monopole antennas based respectively on a "conventional" single-layer and a dual-layer mushroom-like EBG structures. This study demonstrates the superiority of the DL-EBG to achieve more compact antennas. Indeed, the size of the EBG unit cell patch is reduced by a factor of ~ 1.827 while maintaining the EBG height

unchanged and the total antenna height (thickness of the EBG + distance between the EBG and the antenna) was also reduced by a factor of 1.81 for the same resonant frequency (1.3 GHz).

Furthermore, in order to demonstrate the benefit of the DL-EBG, the antenna performances were simulated in three following cases.

- The "bent" monopole element is placed over a standard PEC ground plane (PEC_GP) at a distance of $h = \lambda_o/36$.
- The distance between the standard PEC ground plane (PEC_GP) and the radiator element is progressively increased from $h = \lambda_o/36$ (previous case) to $\lambda_o/7$.
- The "bent" monopole element is placed over a dual-layer MTM ground plane (MTM_GP) at a distance of $h = \lambda_o/36$.

In the first case, the antenna behaves like a capacitor element. In the second case, a height of at least $h = \lambda_o/7$ has been required to achieve good matching impedance and antenna's gain. In the third case, a height of only $h = \lambda_o/36$ is required to obtained comparable results. The study is developed in Sections 4 and 5.

Besides, an array antenna, composed by two identical MTM "bent" monopole antennas placed on both sides of a thin slab of composite material, has been built to form a "Sabre-Type" antenna (Fig. 1). The experimental radiation patterns show a monopole-type antenna behavior with a vertically polarization (VP) and almost-omnidirectional radiation patterns.

The simulations were performed using CST STUDIO SUITE$^{\text{TM}}$ which is based on the Finite Integration Technique (FIT) with a hexahedral meshing grid system for an accurate modeling of metamaterial antenna structures.
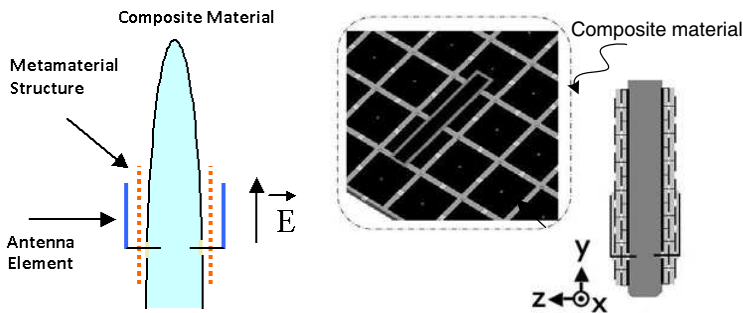

Figure 1. Designed "Sabre-type" antenna with two identical metamaterial-based antennas on both sides of a thin composite material slab.

2. METAMATERIAL ANTENNA DESIGN AND TOPOLOGY

Figure 2 shows the designed MTM-based "bent" monopole antenna which is composed of two parts:

1) A strip line radiating element (length of $0.5\lambda_g$, width of $0.05\lambda_g$) printed on a Rogers 5880LZ dielectric substrate (relative permittivity $\varepsilon_r = 1.96$, loss-tangent $\tan(\delta) = 0.0019$). The dimensions of the dielectric substrate are $0.39\lambda_o \times 0.064\lambda_o$, $\times 0.0055\lambda_0$.

   λ_o is the free space wavelength at $1.3\,\text{GHz}$ and λ_g is the guided wavelength (1):

$$\lambda_g = \lambda_o/\sqrt{\varepsilon_r} \qquad (1)$$

2) a dual-layer mushroom-like EBG (DL-EBG) ground plane composed by 7×7 unit cells with a total height $H = 0.022\lambda_o$ ($\sim \lambda_o/45$) and square lateral sizes of $1.15\lambda_o \times 1.15\lambda_o$. Table 1 summarizes the dimensions of the structure.

The printed "bent" monopole element is fed by a $50\,\Omega$ input coaxial line (as shown by Fig. 2(b)). The position (X, Y) of the feeding input
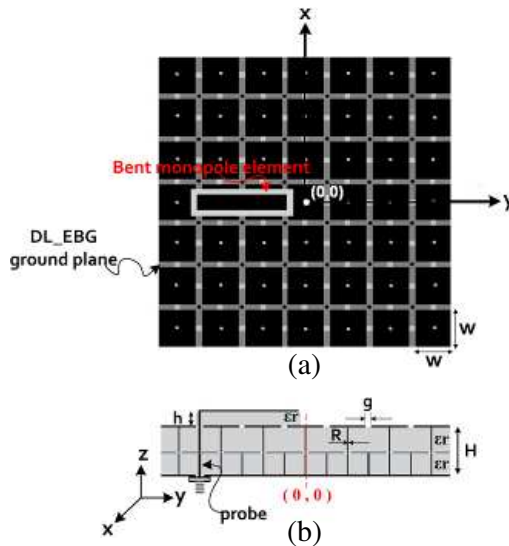

Figure 2. Designed MTM-based "bent" monopole antenna. (a) Top view and (b) side view with the DL-EBG topology and the coordinate's position of the feeding coaxial input.

Table 1. Dimensions for DL-EBG structure.

Name	Symbol	Dimension
metallic square patch	$W \times W$	$0.15\lambda_o \times 0.15\lambda_o$
distance of adjacent metal patches	g	$0.02\lambda_o$
Vias Radius	R	$0.005\lambda_o$
dielectric substrate half height	$H/2$	$0.011\lambda_o$
dielectric relative permittivity	$(\varepsilon_r, \tan\delta)$	$(1.96, 0.0019)$

is carefully determined by the full wave simulations. The optimized coordinates are $X = 0$ and $Y = -0.425\lambda_o$ equivalent to 2.5 unit cells (Fig. 2).

3. ADVANTAGES OF THE DL-EBG STRUCTURE

As mentioned before, two "bent" monopole antennas based on single layer EBG and DL-EBG structures (square patch mushroom-like unit cell) have been simulated and their performances are analyzed.

The two antennas are designed to operate at 1.3 GHz. Here, we choose a dielectric substrate Rohacell 31HF with a permittivity of 1.046, loss tangent $\tan(\delta) = 0.002$ (similar to the air) and a height of $\lambda_{1.3\,\mathrm{GHz}}/42.7$ (for both EBGs). The unit cell (UC) is the mushroom-like patch with a square surface $Ws \times Ws$ [13–16]. Hence, the parameters $(Ws, gs, P, da, de$, Fig. 3) of the two antennas are optimized separately to achieve a resonant frequency at 1.3 GHz while maintaining the same height ($de = 0.023\lambda_0$) and the same length of the "bent" monopole ($La = 0.5\lambda_0$) for the two EBG antenna structures.

Figure 3 shows the designed antennas. In Fig. 3(a) the "bent" monopole is placed over a "conventional" EBG structure [17–21] and in Fig. 3(b), the "bent" monopole is placed over a DL-EBG structure. Fig. 4 gives the simulated reflection coefficient S_{11} for the two antennas for different total height ($D_{\mathrm{total}} = da + de$). Here, da is the distance between the EBG and the antenna element and de is the thickness of the EBG.

Figure 4(a) shows the results of the "bent" monopole antenna based on the "conventional" EBG structure using the optimized parameters of Table 2. The resonant frequency is centered on $\sim 1.3\,\mathrm{GHz}$ and remains unchanged with the distance da. A good matching impedance ($S_{11} < -28\,\mathrm{dB}$) is obtained only for $da = 0.03\lambda_{1.3\,\mathrm{GHz}}$ (or $D_{\mathrm{total}} = 0.053\lambda_{1.3\,\mathrm{GHz}}$).

Figure 4(b) shows the simulated S_{11} parameter of the antenna
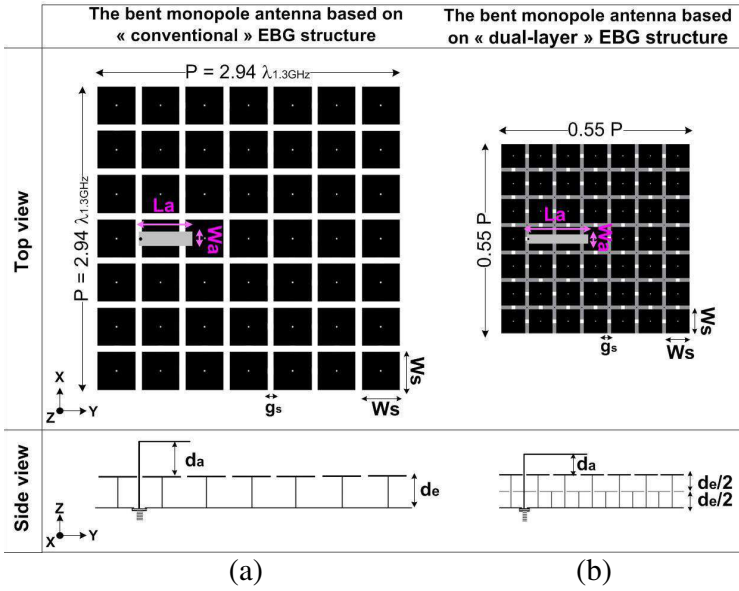
Figure 3. Geometry of the "bent" monopole antenna with two types of EBG structure: (a) "Conventional" mushroom-like EBG structure and (b) "dual-layer" mushroom-like EBG structure.
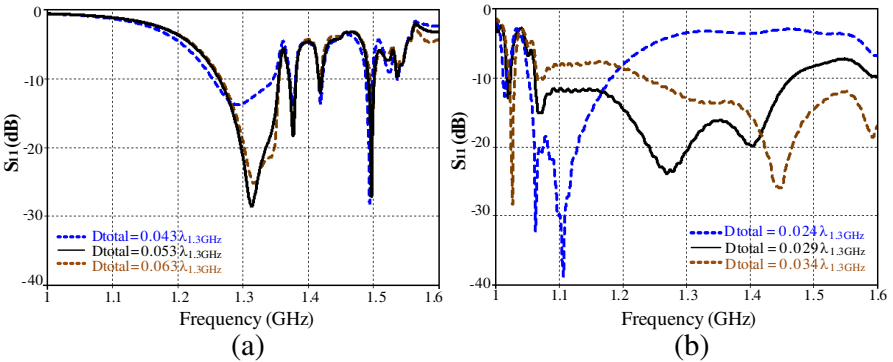

Figure 4. Comparisons of the simulated reflection coefficient S_{11} of the two antennas. (a) "Conventional" mushroom-like EBG structure ($D_{\text{total}} = da + 0.023\lambda_{1.3\,\text{GHz}}$); $da/\lambda_{1.3\,\text{GHz}} = 0.02$, 0.03, 0.04 and (b) dual-layer mushroom-like EBG structure with different antenna height ($D_{\text{total}} = da + 0.023\lambda_{1.3\,\text{GHz}}$); $da/\lambda_{1.3\,\text{GHz}} = 0.001$, 0.006, 0.011.

Table 2. Comparison of the two MTM antenna's dimensions.

Name	"Conventional" mushroom-like EBG structure	Dual layer mushroom-like EBG structure
"Bent" monopole $(La \times Wa)$	$0.5\lambda_{1.3\,\mathrm{GHz}} \times 0.1\lambda_{1.3\,\mathrm{GHz}}$	$0.5\lambda_{1.3\,\mathrm{GHz}} \times 0.06\lambda_{1.3\,\mathrm{GHz}}$
Lateral Surface	$2.94\lambda_{1.3\mathrm{GHz}} \times 2.94\lambda_{1.3\,\mathrm{GHz}}$	$1.62\lambda_{1.3\,\mathrm{GHz}} \times 1.62\lambda_{1.3\,\mathrm{GHz}}$
The overall antenna height $(D_{\text{total}} = da + de)$	$0.053\lambda_{1.3\,\mathrm{GHz}} =$ $0.03\lambda_{1.3\,\mathrm{GHz}} + 0.023\lambda_{1.3\mathrm{GHz}}$	$0.029\ \lambda_{1.3\,\mathrm{GHz}} =$ $0.006\lambda_{1.3\mathrm{GHz}} + 0.023\lambda_{1.3\,\mathrm{GHz}}$
Parameter of EBG structure	"Conventional" mushroom-like EBG structure	Dual layer mushroom-like EBG structure
Ws	$0.4\lambda_{1.3\,\mathrm{GHz}}$	$0.21\lambda_{1.3\,\mathrm{GHz}}$
gs	$0.02\lambda_{1.3\,\mathrm{GHz}}$	$0.02\lambda_{1.3\,\mathrm{GHz}}$
r	$0.005\lambda_{1.3\,\mathrm{GHz}}$	$0.005\lambda_{1.3\,\mathrm{GHz}}$

based on the DL-EBG structure. The antenna has good impedance matching for the all the heights (see the dimensions, Fig. 4) and shows a particularly large bandwidth for $da = 0.006\lambda_{1.3\,\mathrm{GHz}}$ (or $D_{\text{total}} = 0.029\lambda_{1.3\,\mathrm{GHz}}$) which represents 1/5 of the previous distance obtained for the antenna based on the single-layer EBG structure.

Table 2 gives the optimized dimensions for both the two MTM antennas. The advantage of the DL-EBG structure is demonstrated by the reduction of the total antenna height ($D_{\text{total}} = da + de$) and the surface size of the unit cell ($P \times P$) by a factor of 1.8 (see Table 2).

4. STUDY OF THE DL-EBG STRUCTURES

Let's come back to the designed antenna presented in Section 2. The antenna is made more compact by using a dielectric substrate (available Rogers 5880LZ).

Figure 5 gives the conventional EBG unit cell including a ground plane, a dielectric substrate and a metallic patch connected to the ground plane by a metallic vias [22, 23, 25]. The structure can be described by an equivalent shunt combination of inductor and capacitor (lumped LC equivalent circuit). L is associated to the inductive loop path formed by the metallic patches, the vias and the ground plane. C is due to the fringing capacitance.

The resonant frequency can be calculated using the standard formula (2) [22]:

$$f_o = \frac{1}{2\pi\sqrt{LC}} \tag{2}$$

For the fringing capacitor, one of the many reported approximate expressions [22, 23] is that given by Equation (3) in [24]. It allows obtaining more accurate value for the antenna's resonant frequency (2).

$$C_f \approx \frac{\varepsilon_o\varepsilon_r W(2W + g)}{4\pi g} \tag{3}$$

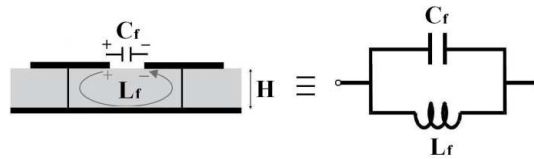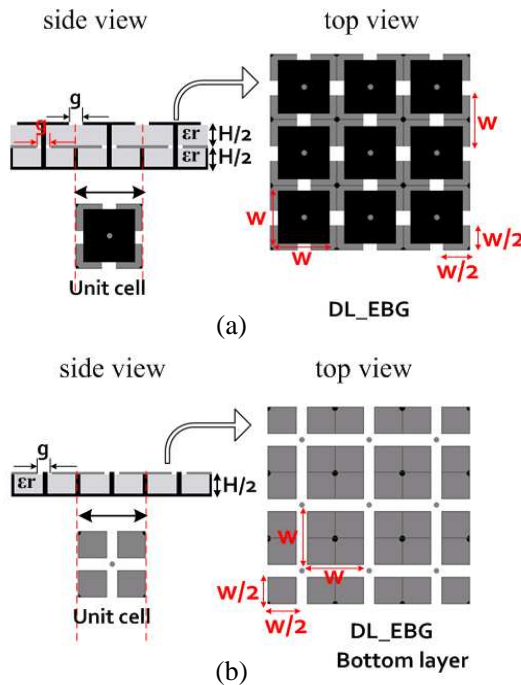The inductor's formula is given by the Equation (4) [25].

$$L = \mu_o\mu_r h \tag{4}$$

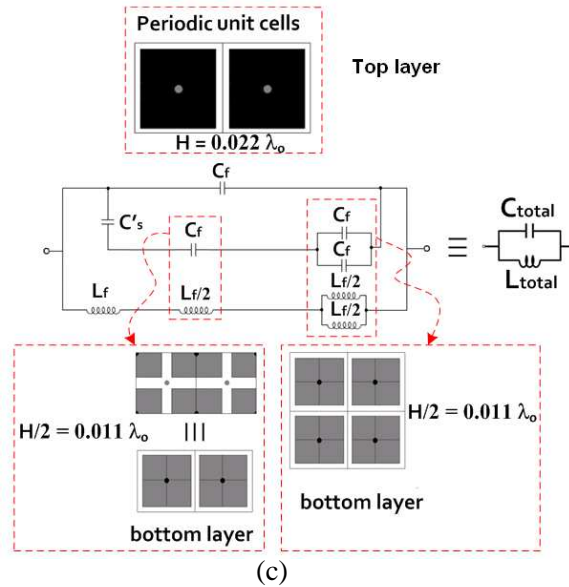**Figure 5.** Mushroom-like EBG structure and its equivalent lumped *LC* elements model.

Figure 6. Dual-layer mushroom-like EBG structure (with distinct metallic vias for each EBG layer). (a) Top view, (b) horizontal cut to view the first EBG layer and (c) the equivalent lumped LC elements model.

Table 3. Calculated L, C and f values of the EBG structure shown in Fig. 5.

• $C_f = 0.7\,\text{pF}$ (3)	• $C_{\text{total}} = 1.13\,\text{pF}$ (7)	• $f_0 = 1.4\,\text{GHz}$ (2)
• $C'_s = 6.1\,\text{pF}$ (5)	• $L_{\text{total}} = 1.75 \times L_f = 11\,\text{nH}$ (4)	
• $L_f = 6.3\,\text{nH}$ (4)		

The DL-EBG structure proposed first by the author Y. Rahmat-Samii [22] and developed in [26, 27] is shown in Fig. 6. The metallic vias are distinct for each mushroom-like EBG layer.

The structure can be described also by an equivalent parallel LC lumped element as shown by Fig. 6(c) [23–25]. Here C'_s the parallel-plate capacitor which expression can be calculated using the Equation (5), where A_e is the "overlapping" area of the metallic patches given by Equation (6). Table 3 gives the calculated LC

parameters (C_{total}, L_{total} and f_0).

$$C'_s = \varepsilon_0 \varepsilon_r \frac{4A_e}{H/2} \tag{5}$$

$$A_e = \left(\frac{W-g}{2}\right)^2 \tag{6}$$

$$C_{\text{total}} = C_f + \frac{2C_f C'_s}{2C_f + 3C'_s} \tag{7}$$

Figure 7(a) sketched the suspended transmission line method [28, 29] used here to determine numerically the transmission signal (S_{21}) across the metasurface of Fig. 6(a). Fig. 7(b) displays the simulated S_{21} determined using this setup. The central frequency is centered on $f = 1.35\,\text{GHz}$ and the bandgap (transmission S_{21} below $-10\,\text{dB}$) is about 440 MHz, from 1.08 GHz to 1.51 GHz and corresponding to a fractional bandwidth of 33%. Hence, the simulated resonant frequency is not far from the predicted one (Table 3) using the formulas (2) to (7).
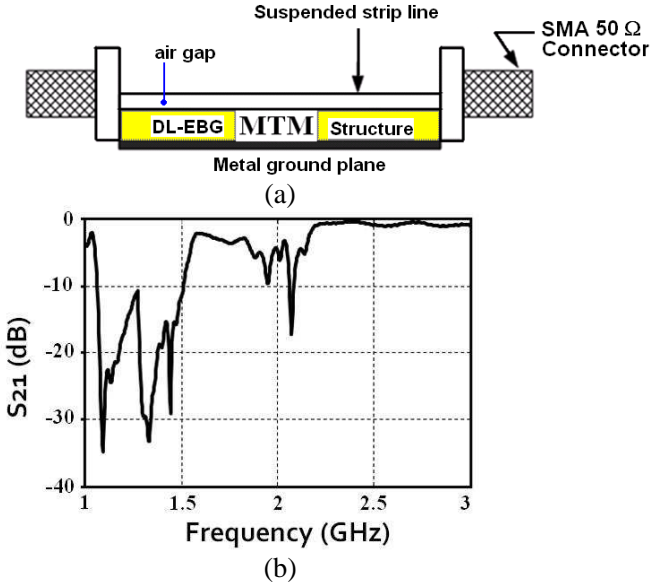

(a)

(b)

Figure 7. (a) Model setup of the suspended transmission line and (b) the simulated transmitted S_{21} parameter, across the metasurface of the Fig. 6(a).

5. ANTENNA INPUT IMPEDANCE: COMPARISON BETWEEN STANDARD METALLIC GROUND PLANE AND METAMATERIAL DL-EBG GROUND PLANE

In this section, the "bent" monopole antenna is simulated respectively in the three following cases:

Case 1: with a standard metallic ground plane (PEC) and a total height of $\lambda_o/36$ (PEC_GP, $\lambda_o/36$)

Case 2: with a standard metallic ground plane (PEC) and a total height of $\lambda_o/7$ (PEC_GP, $\lambda_o/7$)

Case 3: with a thin metamaterial DL-EBG ground plane and a total height of $\lambda_o/36$ (MTM_GP, $\lambda_o/36$).

In order to compare the different simulation results, some parameters remain unchanged; here the finite size of the ground plane ($1.15\lambda_o \times 1.15\lambda_o$), the "bent" monopole element (dimensions and material) and the coaxial feeding position ($X = 0$, $Y = -0.425\lambda_o$).

Figure 8 gives the input impedance (Smith chart) referenced to $50\,\Omega$ for the three studied cases. For the first case, the input impedance becomes more and more capacitive when the frequency increase and the antenna cannot be matched to $50\,\Omega$. For the second case, the input impedance crosses the matching circle ($50\,\Omega$) at $f = 1.3\,\text{GHz}$. For the third case, the input impedance forms a loop around $f = 1.3\,\text{GHz}$ and the antenna may be matched over a large bandwidth from $1.193\,\text{GHz}$ to $1.517\,\text{GHz}$ (see also Fig. 9(b)). The relative bandwidth is near 23.9% in good agreement with the calculated value; 26% using the formula (8) and LC values in the Table 3.
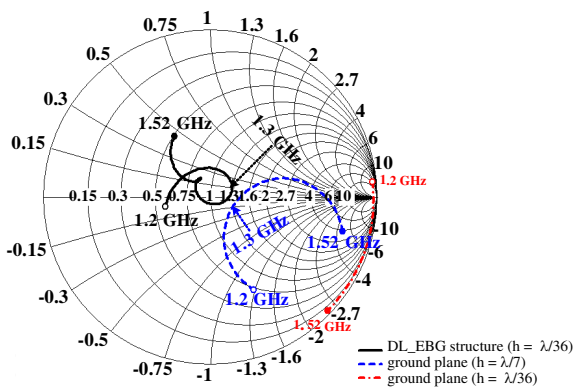

Figure 8. Reflection coefficient (Smith chart) of the "bent" monopole antenna for the three studied cases.
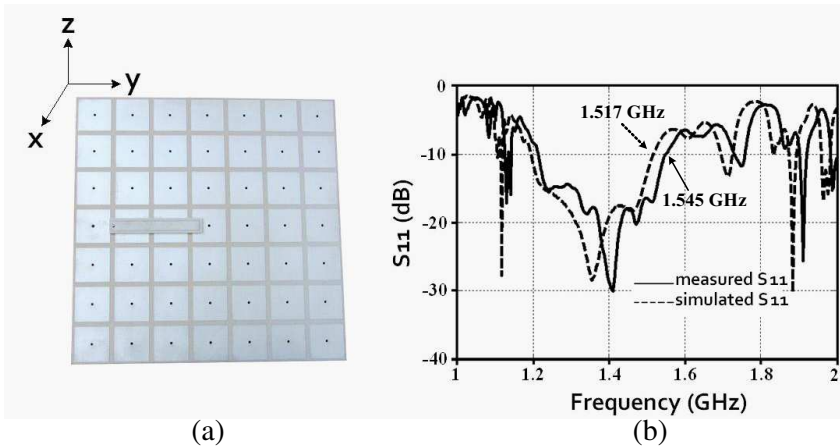
Figure 9. (a) Metamaterial fabricated prototype antenna, (b) measured and simulated antenna's S_{11} parameter.

Table 4. The input impedance and the reflection coefficient (S_{11}, dB) in the Case 3.

Frequency GHz	1.2	1.3	1.305	1.4	1.5
S_{11}, dB	−11	−19	−19	−18	−12
input impedance, Ω	$28.82-j2.2$	$62.17+j1.76$	$61.28+j0$	$40.5+j5.2$	$33.4+j9.25$

The radiation bandwidth [30] is given by Equation (8):

$$BW = \frac{Z_S}{\eta_0} = \frac{\sqrt{\frac{L}{C}}}{\eta_0} \qquad \eta_0 = 377\,\Omega \tag{8}$$

Table 4 summarizes the antenna's input impedance and the reflection coefficient (S_{11} dB) for different frequencies inside the bandwidth which goes from $1.2\,\text{GHz}$ to $1.52\,\text{GHz}$.

6. METAMATERIAL ANTENNA: PROTOTYPE MEASUREMENTS

The fabricated antenna prototype is shown Fig. 9(a) with overall sizes of $1.15\lambda_o \times 1.15\lambda_o \times 0.027\lambda_o$. Fig. 9(b) shows a comparison of the simulated and the measured magnitude of the antenna's reflection coefficient S_{11}. The agreement between the measured and simulated results is remarkable. The measurement gives a resonant frequency at $1.4\,\text{GHz}$ and a bandwidth frequency from $1.212\,\text{GHz}$ to $1.55\,\text{GHz}$ and a fractional bandwidth of 24.4%. The simulation result gives a resonant

frequency of 1.35 GHz and a bandwidth which goes from 1.193 GHz
to 1.517 GHz (23.9%). The main difference is due to the slightly
shift of the resonant frequency ($\sim$ 30 MHz). Those results allow us
to validate the simulation model of the metamaterial-based antenna.
We must notice that any neither fitting nor parasitical elements due
to the fabrication process were taken into account in the numerical
calculations.

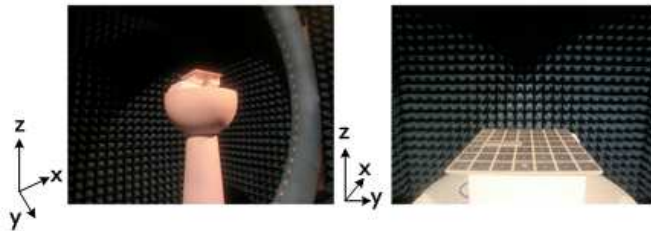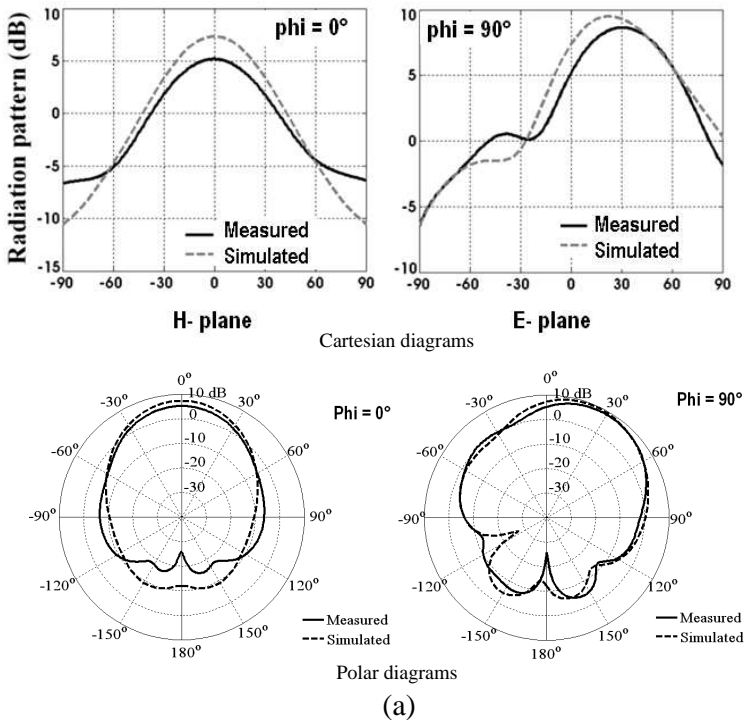The radiation patterns measurements are performed with the

Figure 10. StarLab anechoic chamber of SATIMO; Measurement of
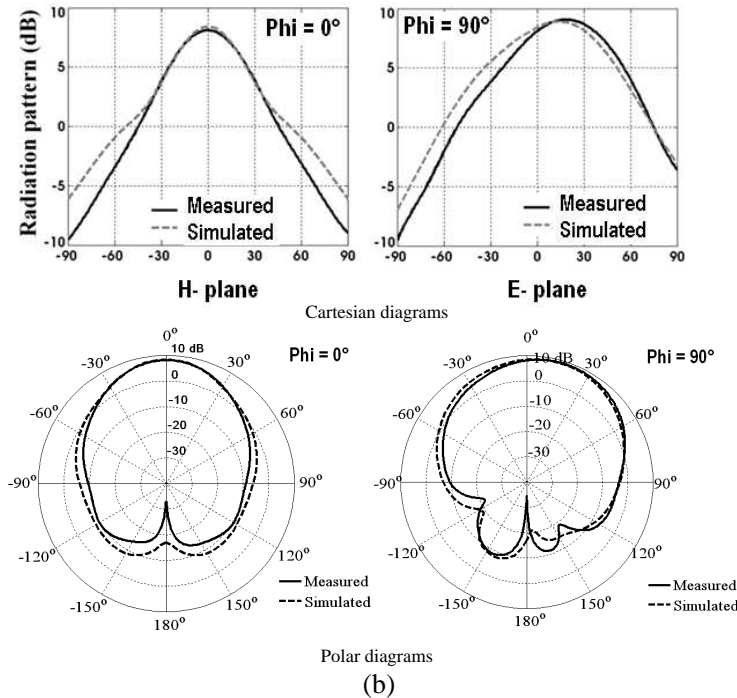the MTM antenna's radiation patterns.

(a)

Figure 11. Measured and simulated radiation patterns (Cartesian and polar) in the H-plane (Phi $= 0°$) and the E-plane (Phi $= 90°$) at (a) $f = 1.35\,\text{GHz}$ and (b) $f = 1.45\,\text{GHz}$.

StarLab (Fig. 10) SATIMO anechoic chamber facilities.

Figure 11 gives the E and H planes radiation patterns (Cartesian and polar diagrams) for the central frequencies $f = 1.35\,\text{GHz}$ and $f = 1.45\,\text{GHz}$. At 1.35 GHz, the antenna's gain is about 5 dB at $\theta = 0°$ and 8.5 dB at $\theta = 30°$ (Fig. 11(a)). At 1.45 GHz, the measured maximum gain is about 8 dB at $\theta = 0°$ and 9 dB at $\theta = 17°$ (Fig. 11(b)). The observed differences are due to the frequency offset between the measurement and simulation (Fig. 9(b)). It should be noted that the radiation diagrams are identical in measurement and simulation, if we take into account the frequency shift.

Figure 12 gives the radiations patterns (Cartesian diagrams) for the band edge frequencies (at $S_{11} = -10\,\text{dB}$). The left frequency is $f = 1.215\,\text{GHz}$ identical (as shown in Fig. 9(b)) for the measured and simulated S_{11}. The right band edge frequency is in contrast not the same (shift of 50 MHz) and $f = 1.545\,\text{GHz}$ for the measured S_{11} and $f = 1.517\,\text{GHz}$ for the simulated S_{11} (Fig. 9(b)).

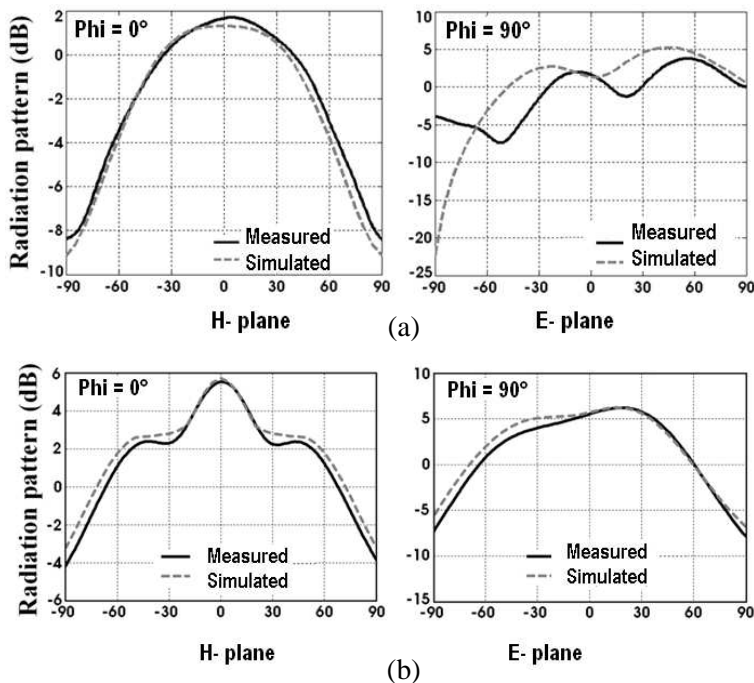**Figure 12.** Measured and simulated radiation patterns (Cartesian) the H-plane (Phi $= 0°$) and the E-plane (Phi $= 90°$) at (a) $f = 1.215$ GHz and (b) $f = 1.545$ GHz (measurement) and $f = 1.517$ GHz (simulation).

At 1.215 GHz, the antenna's the measured maximum gain is around 2 dB at $\theta = 0°$ (Fig. 12(a)). At 1.545 GHz, the measured maximum gain is about 6 dB at $\theta = 0°$ (Fig. 12(b)).

7. "SABRE" ANTENNA: EXPERIMENTAL CHARACTERIZATIONS

A "Sabre-type" antenna composed by two identical "bent" monopole antennas (as shown in Fig. 1) has been built and totally characterized. In order to achieve a vertically polarized (VP) and omnidirectional radiation patterns, the two DL-EBG MTM based antenna elements are placed on both sides of a composite material slab (thickness of about 3 mm). The "Sabre-type" antenna is fed by a 50 Ω coaxial line (50 Ω SMA input connector) which use two quarter-wavelength impedance transformers — type circuits (Fig. 13) to match the two 50 Ω input
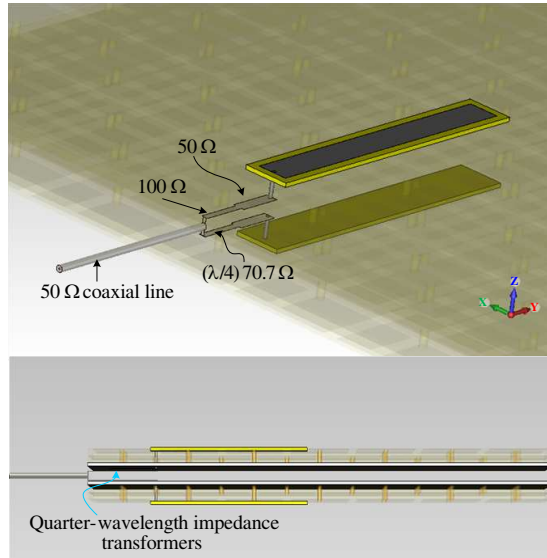
Figure 13. Designed feeding circuit for $50\,\Omega$ feeding input "Sabre-type" antenna. Two quarter-wavelength impedance transformers circuits are used to match the bent monopole elements.
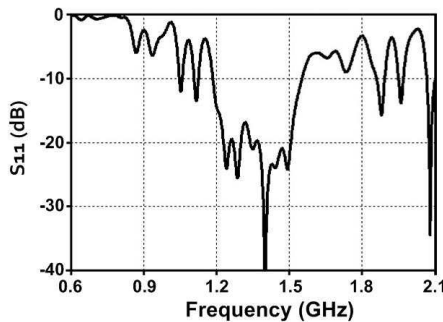

Figure 14. Simulated reflection coefficient S_{11} of the proposed "Sabre-type" antenna.

impedance of the bent monopoles placed on both sides of the composite slab.

The total S_{11} characteristics versus frequency of "Sabre-type" antenna have been simulated and the result is presented in Fig. 14. The resonant frequency is around $1.36\,\text{GHz}$ with good matching impedance ($S_{11} < -20\,\text{dB}$) from $1.197\,\text{GHz}$ to $1.531\,\text{GHz}$ (or 23.9%).
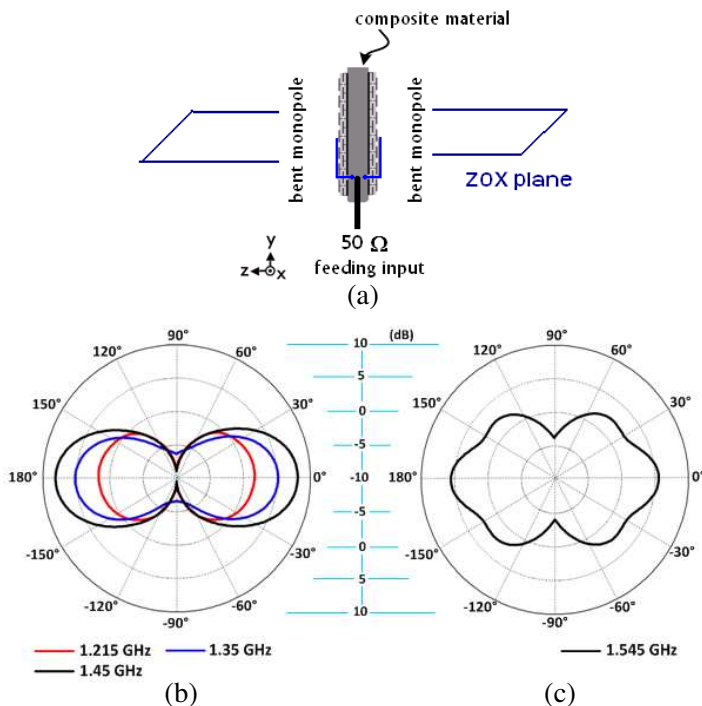
Figure 15. (a) Definition of the azimuthally-plane and (b) and (c) radiation patterns of the "Sabre" antenna (Fig. 1), (b) for 1.215 GHz (red curve), 1.35 GHz (blue curve) and 1.45 GHz (black curve) and (c) for 1.545 GHz (black curve).

Table 5. "Sabre-type" antenna maximum and minimum gain versus frequency.

Frequency GHz	1.215	1.35	1.450	1.545
Gain maximum, dB ($\theta = 0°$)	+2	+5	+8.5	+5

The radiation patterns of the "Sabre-type" antenna in the azimuthal plane are shown on Fig. 15 for the four previous selected frequencies ($f = 1.215$-, 1.35-, 1.45- and 1.545 GHz). The "Sabre-type" antenna behaves like a monopole-type VP antenna in all the bandwidth frequency. The radiation patterns are almost directive with a highest gain at 1.45 GHz. Table 5 gives the maximum gain for each frequency.

8. PARAMETRICAL STUDIES

Some sensitive parameters such as the length of the "bent" monopole antenna, the position of the feeding coaxial input and the metamaterial surface area (number of the unit cells) are analyzed in this section and compared to the optimum solution.

8.1. "Bent" Monopole's Length

Figure 16 shows the simulated reflection coefficient (magnitude of S_{11}) when the length of the "bent" monopole antenna varies from $0.3\lambda_0 = 70$ mm (or $0.42\lambda_g$) to $0.546\,\lambda_0 = 126$ mm (or $0.76\lambda_g$) while the others antenna's parameters are maintained constant. The antenna's operating frequency decrease when the length increases. The matching impedance bandwidth has an optimum value for $\sim \lambda_g/2$ (86 mm $= 0.373\lambda_0$) centered on 1.3 GHz.

8.2. "Bent" Monopole Position

Figure 17 shows the simulation results of the S_{11} reflection coefficient when the coordinates (X, Y) of the feeding input move from the initial position, situated at the left edge of the DL-EBG ground plane, in the direction of its center ($X = 0$, $Y = 0$) and taking the following values:

- Initial position ($X = 0$, $Y = -0.425\lambda_0$) $\Leftrightarrow$ ($X = 0$, $Y = -2.5$ unit cells): Fig. 17 curve (1),
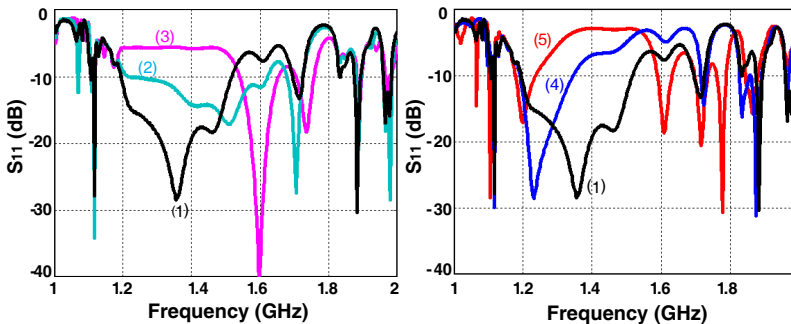

Figure 16. Simulated reflection coefficient S_{11} (dB) of the MTM antenna when the length (L) of the printed "bent" monopole element takes the following values: (1) $L = 0.5\lambda_g$, (2) $L = 0.48\lambda_g$, (3) $L = 0.42\lambda_g$, (4) $L = 0.64\lambda_g$ and (5) $L = 0.76\lambda_g$.

- Second Position ($X = 0$, $Y = -0.255\lambda_0$) $\Leftrightarrow$ ($X = 0$, $Y = -1.5$ unit cells): Fig. 17 curve (2),
- Third position ($X = 0$, $Y = -0.085\lambda_0$) $\Leftrightarrow$ ($X = 0$, $Y = -0.5$ unit cell): Fig. 17 curve (3).

The simulated results show poor antenna matching impedance's for the two last feeding inputs (Fig. 17 curve (2) and curve (3)).

8.3. DL-EBG MTM-ground Plane Size (Numbers of the Unit Cells)

Figure 18 depicts the reflection coefficient (S_{11}) simulated for a variable number of unit cells ($N \times N$) which form the DL-EBG-GP surface, here N varies from $N = 4$ to $N = 7$. The surface of (4×4) unit cells or a square size of $0.68\lambda_o \times 0.68\lambda_o$ behaves like a director-plane and not as a ground plane and the antenna is not adapted. In contrast, the (5×5) unit cells or a square size of $0.85\lambda_o \times 0.85\lambda_o$ good matching impedance is achieved with a large bandwidth; from 1.1 GHz to 1.52 GHz which confirm the well known minimum size for the ground plane equal to $0.8\lambda_o \times 0.8\lambda_o$. Good input matching impedance is obtained also for the case (6×6) unit cells or a square size of $1.02\lambda_o \times 1.02\lambda_o$ for the EBG_GP. The bandwidth; $S_{11} < -10$ dB goes from 1.16 GHz to 1.52 GHz which corresponds to a fractional bandwidth of more than 26.8%. This is the raison we choice a DL-EBG ground plane surface of 7×7 unit cells or $1.15\lambda_o \times 1.15\lambda_o$.
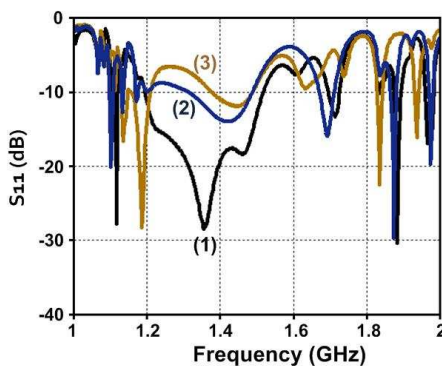

Figure 17. Simulated reflection coefficient when the position of the feeding input varies; (1) Initial position ($X = 0$, $Y = -0.425\lambda_0$), (2) second position ($X = 0$, $Y = -0.255\lambda_0$) and (3) third position ($X = 0$, $Y = -0.085\lambda_0$).
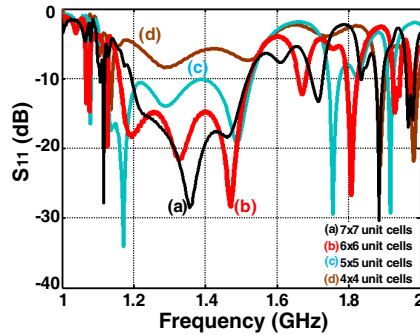
Figure 18. Comparisons of S_{11} for different sizes of the DL-EBG structure; (a) for (7×7), (b) for (6×6), (c) for (5×5) and (d) for (4×4) Unit Cells.

9. CONCLUSION

In this paper, we propose a detailed study of low-profile (only $\lambda_o/36$) "bent" monopole MTM-based antenna with a dimension of $1.15\lambda_o \times 1.15\lambda_o \times 0.027\lambda_o$ at 1.3 GHz. The MTM ground plane is dual-layer mushroom-like EBG structure (DL-EBG). For the same operating frequency and the same height, the simulation results show that the DL-EBG structure can achieve wider bandgap than the "conventional" mushroom-like EBG structure by a factor 4 at least (respectively 33% and 8%). A prototype MTM-based antenna has been fabricated and fully characterized. The measurements show a resonant frequency around 1.4 GHz and a fractional bandwidth of 24.4%. A remarkable agreement between the measurement and the simulations are obtained. Moreover, an array of two identical monopole antennas (placed on both sides of a thin composite media) has been built to form a "Sabre-type" antenna. The numerical and measured results demonstrate a vertically polarization of the "sabre" antenna which behaves like a standard monopole. The radiation patterns in the elevation plane are quasi-omnidirectional quite identical to those of a standard of monopole type antenna. In the azimuth plane the radiation patterns are more directional with a maximum gain of 8.7 dB at 1.45 GHz. Parametrical studies with some sensitive parameters such as the number of MTM unit cells (lateral surface) of the ground plane, the dimension of the radiator element and the position of the feeding antenna input have been presented. In summary, we proposed an antenna based on a dual-layer EBG structure with the following original features; more compact for low operating frequency (1.3 GHz), experimental bandwidth of 24.4%, total height is $0.027\lambda_{1.3\,\text{GHz}}$ and very good return loss of 30 dB.

ACKNOWLEDGMENT

REFERENCES

1. Sievenpiper, D., "Low-profile antenna," U.S. Patent 7050003, May 23, 2006.

2. Hansen, R. C., *Electrically Small, Superdirective, and Superconducting Antennas*, 82–89, New Jersey, 2006.

3. Hoorfar, A., "An experimental study of microstrip antennas on very high permittivity ceramic substrates and very small ground planes," *IEEE Trans. Antennas Propagation*, Vol. 49, No. 5, 838–840, May 2001.

4. Olaode, O. O., "Characterization of meander dipole antennas with a geometry based, frequency-independent lumped element model," *IEEE Antennas and Wireless Propagation Letters*, Vol. 11, 346–349, 2012.

5. Ares-Pena, F. J., "Genetic algorithms in the design and optimization of antenna array patterns," *IEEE Trans. Antennas Propagation*, Vol. 47, No. 3, 506–510, March 1999.

6. Sievenpiper, D., L. Zhang, R. F. Jimenez Broas, N. G. Alexópolous, and E. Yablonovitch, "High-impedance electromagnetic surfaces with a forbidden frequency band," *IEEE Transactions on Microwave Theory and Techniques*, Vol. 47, No. 11, November 1999.

7. Sievenpiper, D., J. Colburn, B. Fong, M. Ganz, M. Gyure, J. Lynch, J. Ottusch, and J. Visher, "Artificial impedance surface," U.S. Patent 7830310, November 9, 2010.

8. Yang, F. and Y. Rahmat-Samii, "Reflection phase characterizations of the EBG ground plane for low profile wire antenna applications," *IEEE Trans. Antennas Propagation*, Vol. 51, No. 10, 2691–703, 2003.

9. Rahman, M. and M. Stuchly, "Wide-band microstrip patch antenna with planar PBG structure," *Proc. IEEE APS Dig.*, Vol. 2, 486–9, 2001.

10. Tran, C. M., H. H. Ouslimani, L. Zhou, and A. C. Priou, "High impedance surfaces based antennas for high data

rate communications at 40 GHz," *Progress In Electromagnetic Research C*, Vol. 13, 217–229, 2010.

11. Yang, F., A. Aminian, and Y. Rahmat-Samii, "A low profile surface wave antenna equivalent to a vertical monopole antenna," *IEEE APS Int. Symp. Dig.*, Vol. 2, 1939–42, Monterey, CA, June 20–26, 2004.

12. Yang, F. and Y. Rahmat-Samii, "Bent monopole antennas on EBG ground plane with reconfigurable radiation patterns," *IEEE APS Int. Symp. Dig.*, Vol. 2, 1819–1822, Monterey, CA, June 20–26, 2004.

13. Yang, F. and Y. Rahmat-Samii, "Polarization dependent electromagnetic band gap (PDEBG) structures: Designs and applications," *Microwave Optical Tech. Lett.*, Vol. 41, No. 6, 439–44, 2004.

14. Gonzalo, R., P. Maagt, and M. Sorolla, "Enhanced patch-antenna performance by suppressing surface waves using photonic-bandgap substrates," *IEEE Trans. Microwave Theory Tech.*, Vol. 47, 2131–2138, 1999.

15. Tavallaee, A. and Y. Rahmat-Samii, "A novel strategy for broadband and miniaturized EBG designs: Hybrid MTL theory and PSO algorithm," *IEEE APS Int. Symp. Dig.*, 161–164, June 2007.

16. Cheng, H. R. and Q. Y. Song, "Design of a novel EBG structure and its application in fractal microstrip antenna," *Progress In Electromagnetics Research C*, Vol. 11, 81–90, 2009

17. Rahmat-Samii, Y. and H. Mosallaei, "Electromagnetic band-gap structures: Classification, characterization and applications," *Proceedings of IEE-ICAP Symposium*, 560–564, April 2001.

18. Qu, D., L. Shafai, and A. Foroozesh, "Improving microstrip patch antenna performance using EBG substrates," *IEE Proc. Microwaves, Antennas Propagation*, Vol. 153, No. 6, 558–563, 2006.

19. Kildal, P.-S., "Artificially soft and hard surfaces in electromagnetics," *IEEE Trans. Antennas Propagation*, Vol. 38, No. 10, 1537–1544, 1990.

20. De Maagt, P., R. Gonzalo, Y. C. Vardaxoglou, and J.-M. Baracco, "Electromagnetic band gap antennas and components for microwave and (sub) millimeter wave applications," *IEEE Trans. Antennas Propagation*, Vol. 51, No. 10, 2667–2677, 2003.

21. Azad, M. Z. and M. Ali, "Novel wideband directional dipole antenna on a mushroom like EBG structure," *IEEE Trans.*

Antennas Propagation, Vol. 56, 1242–1250, May 2008.

22. Yang, F. and Y. Rahmat-Samii, *Electromagnetic Band Gap Structures in Antenna Engineering*, Chapter 3, 59–61, 2009.

23. Zhao, Y., Y. Hao, and C. G. Parini, "Radiation properties of PIFA on electromagnetic bandgap substrates," *Microwave and Optical Technology Letters*, Vol. 44, No. 1, January 5, 2005.

24. Fogiel, M. and J. J. Molitoris, *The Physics Problem Solver*, Université de l'État de Pennsylvanie, 2000.

25. Ghosh, S., T.-N. Tran, and T. Le-Ngoc, "A dual-layer EBG-based miniaturized patch multi-antenna structure," *IEEE International Symposium on Antennas and Propagation (APSURSI)*, 1828–1831, July 2011.

26. Azarbar, A. and J. Ghalibafan, "A compact low-permittivity dual-layer EBG structure for mutual coupling reduction," *International Journal of Antennas and Propagation*, Vol. 2011, Article ID 237454, June 2011.

27. Boisbouvier, N., A. Louzir, F. Le Bolzer, A.-C. Tarot, and K. Mahdjoubi, "A double layer EBG structure for slot-line printed devices," *IEEE Antennas and Propagation Society International Symposium*, Vol. 4, 3553–3556, June 2004.

28. Zhang, L.-J., C.-H. Liang, L. Liang, and L. Chen, "A novel design approach for dual-band electromagnetic band-gap structure," *Progress In Electromagnetics Research M*, Vol. 4, 81–91, 2008.

29. Yang, L., M. Fan, F. Chen, J. She, and Z. Feng, "A novel compact electromagnetic-bandgap (EBG) structure and its applications for microwave circuits," *IEEE Transactions on Microwave Theory and Techniques*, Vol. 53, No. 1, January 2005.

30. Sievenpiper, D. F., "High-impedance electromagnetic surfaces," Ph.D. Dissertation at University of California, Chapter 3, 28–30, Los Angeles, 1999.